RESEARCH PAPER

CrossMark

Design and fabrication of inverted tapered micro-pillars for spontaneously transporting liquid upward

Yun Chen[1,2,3,5] · Dachuang Shi[1,2] · Xiquan Mai[1,2] · Liyi Li[3] · Jian Gao[1,2] · Xin Chen[1,2] · Han-Xiong Li[4] · Ching-Ping Wong[3,5]

Abstract

Directional liquid transport has significant domestic and industrial applications. Theoretically, tapered objects can transport a liquid droplet horizontally or along a small slant angle: Many biomaterials have already demonstrated this ability. However, spontaneously transporting liquid in the vertical direction has been challenging. In this study, a numerical model was developed to simulate the transporting process and design inverted tapered pillars. The range of acceptable parameters for the pillar's geometry was obtained. When the taper angle, the diameter of the bottom end of the pillar, and the contact angle of the liquid are less than $10°$, $80\ \mu m$, and $54.5°$, respectively, then liquid may be transported upward spontaneously. An experimental setup for fabricating the pillars was also developed and presented. With this setup, the designed pillars were successfully fabricated by the gradient electrochemical corrosion method and enhanced its wettability by the electrochemical modification method. The fabricated pillars were then experimentally validated, showing that they can spontaneously transport a micrometer-scale droplet upward. These results may provide a new and systematic way to design and fabricate a tool for high-efficiency liquid transport.

Keywords Inverted tapered micro-pillar · Upward liquid transport · Fluid dynamics modeling · Manufacturing technology

1 Introduction

Directional liquid transport has significant domestic and industrial applications, such as in 3D printing (Ferraro et al. 2010; Wu et al. 2015), inkjet printing (Basaran and Suryo 2007), micro-fluidics (Guo et al. 2012), chemistry analysis (Price and Paegel 2016), microelectronic cooling (Chen et al. 2013; Li et al. 2016), and potential new devices (Wang et al. 2015; Park et al. 2016; Katsikis et al. 2015). It is common knowledge that liquid always travels downward due to the force of gravity. It is possible, however, that liquid can overcome gravity and move upward spontaneously—capillary action is such an example (Rowlinson and Widom 2013; Bico and Quéré 2002), but the liquid can only travel inside hollow tubes and it is difficult to transport the liquid to a substrate.

Physicists recently found that theoretically a liquid droplet could travel on a solid surface horizontally or at a small slant angle at high speed due to a wettability gradient (Subramanian et al. 2005; Vorobyev and Guo 2009; Ju et al. 2013), thermal gradient (Dai et al. 2016), curvature gradient (Lorenceau and Quéré 2004; Luo 2015; Li et al. 2013; Huang et al. 2013;

✉ Xin Chen
chenx@gdut.edu.cn

✉ Ching-Ping Wong
cp.wong@mse.gatech.edu

1   School of Electromechanical Engineering, Guangdong University of Technology, Guangzhou 510006, China

2   Key Laboratory of Mechanical Equipment Manufacturing and Control Technology of Ministry of Education, Guangdong University of Technology, Guangzhou 510006, China

3   School of Materials Science and Engineering, Georgia Institute of Technology, Atlanta, GA 30332, USA

4   Department of Systems Engineering and Engineering Management, City University of Hong Kong, Tat Chee Avenue, Kowloon, Hong Kong SAR, China

5   School of Engineering, The Chinese University of Hong Kong, Shatin, Hong Kong

Lv et al. 2014), etc. In particular, for a droplet transported by a curvature gradient, many such biomaterials are found in nature (Ju et al. 2014; Zhu et al. 2016), e.g., a cactus spine (Ju et al. 2012) and spider silk (Zheng et al. 2010). Study of these materials may result in other methods by which fluid can be transported directionally and its movement controlled.

According to the curvature-gradient-driven theory (Lorenceau and Quéré 2004; Luo 2015; Michielsen et al. 2011), when a droplet is resting on an inverted tapered pillar (as shown in Fig. 1a), the upward force arising from the Laplace pressure F_L (pointing from the small end to the big end) can be simplified as (Zhu et al. 2016)

$$F_L = -\int_{R_L}^{R_U} \frac{2\gamma}{(r + r_0)^2} \sin a \, dr. \qquad (1.1)$$

Similarly, the gravity force of the droplet F_G can be written as

$$F_G = \int_{R_L}^{R_U} \rho g * \frac{2\pi r (r + r_0)}{\sin a} dr, \qquad (1.2)$$

where the R_U and R_L are the local radii of the object at the upper and lower sides of the droplet, respectively; γ is the surface tension; r is the local radii of the cone-structured object; r_0 is the thickness of the droplet; ρ is the liquid density; g is the gravity acceleration; a is the half apex angle of the cone; and dr is the minute incremental radius along the cone.

For most common cases, as the object is large, the Laplace pressure F_L is much smaller than the force of gravity F_G, so the droplet always drops downward instead of moving upward. However, if the sizes of the droplet and cone-structured object decrease, both the Laplace pressure F_L and the gravity force F_G decrease correspondingly, but the gravity force F_G decreases faster. This can be partially verified in that a microscale water droplet can be transported on a conical object at a maximum speed of 0.42 m/s, while a nanoscale droplet can theoretically be transported at a high speed of over 100 m/s (Lv et al. 2014). Therefore, it can be inferred that if the sizes of the droplet and cone-structured object are sufficiently small, eventually, the Laplace pressure F_L will exceed the gravity force F_G and the droplet can be transported upward by the inverted tapered pillar, as shown in Fig. 1b.

However, this upward motion is rarely seen. By static finite element simulation, Liang et al. (2015) found that at certain conditions the droplet can achieve stable equilibrium on hydrophilic conical fibers. However, due to the limitations of the algorithm, the dynamic process of transporting water cannot be shown. Li and Thoroddsen (2013) experimentally studied the factors affecting the climbing velocity and found that the speed of the fastest droplets is limited by inertia following their emergence at the cone tip; further, Guo and Tang (2015) experimentally found that cactus spines can transport the liquid droplet upward with a maximum velocity of approximately 1.17 m/s. Being able to eventually design, optimize using simulation models, and fabricate tapered pillars with similar functionality is essential to large-scale fabrication (Chu and Liu 2008; Madou 2011; Li et al. 2015).

In this work, a numerical model was developed to design and optimize the geometry of inverted tapered pillars. An experimental setup was also developed and used to successfully fabricate the resulting pillar design. The fabricated pillar was then experimentally validated by showing that it can transport a micro-size droplet upward spontaneously. This may provide a systematic way to design and fabricate tools for liquid transport in high efficiency.

2 Design of inverted tapered micro-pillars

2.1 Simulation model

An axial symmetry model was developed by using Open-FOAM Extended 1.6, as shown in Fig. 2. The pillar was 1000 μm in length, and its bottom end was 10 μm in diameter while the top end was 65 μm; thus, the taper angle
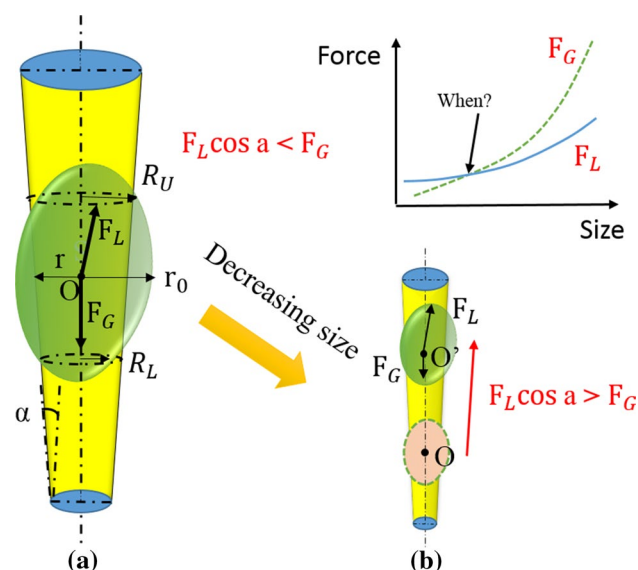
Fig. 1 Transporting a liquid droplet upward by a small inverted tapered pillar. **a** Big pillars cannot transport droplets upward spontaneously; **b** when the size of the pillar is sufficiently small, it can transport droplets upward
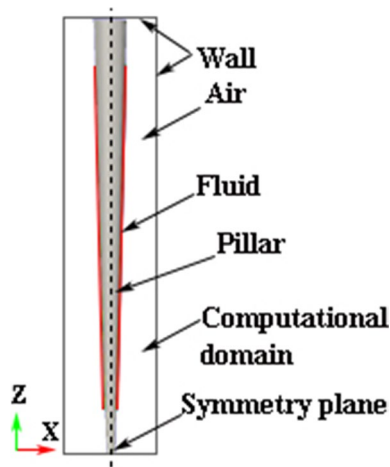
Fig. 2 Section view of the simulation model. The simulation model has axial symmetry: It consists of the pillar, fluid, and air, all of which are surrounded by the wall

Table 1 Key parameters of the simulation model

Parameters	
Diameter of the bottom	10 μm
Diameter of the top	65 μm
Length	1 mm
Taper angle	1.57°
Liquid	Water
Liquid thickness	200 nm
Contact angle	45°
Surface tension	0.073 N/m
Gravity	9.81 m/s^2
Atmosphere pressure	1.01e5 Pa
Volume of liquid	0.02 nL
Width of domain area	100 μm

was 1.57°. As is typical in applications of water collection using inverted tapered micro-pillars, a liquid film was firstly formed on the surface of the pillar (Zheng et al. 2010); then, a layer of liquid with thickness of 200 nm was initially deposited on the surface of the pillar in the model. The volume of the liquid was approximately 0.02 nL. The liquid used in the simulation was water, so the contact angle and surface tension were set as 45° and 0.073 N/m (Yuan and Lee 2013), respectively. Gravity and atmospheric pressure were also considered. The key parameters are listed in Table 1.

2.2 Modeling results and optimization

2.2.1 Modeling results

Figure 3 shows the modeling results. It can be seen that due to the Rayleigh instability, the thin layer of water on the surface of the inverted tapered micro-pillar firstly formed two droplets from 0 to 0.1 ms, and then due to the driving force arising from the shape gradient (Laplace pressure), the droplets were propelled upward toward the region with a larger radius of curvature. As the curvature of the bottom end was larger than that of the top end, so was the driving force; therefore, the lower droplet moved faster than the upper one. The two droplets merged at the middle of the pillar at 0.2 ms, and the newly formed droplet moved slowly from 0.3 to 0.5 ms. It then moved toward the top end at a high speed from 0.6 to 1.1 ms, reaching the top of the computational domain at 1.2–2.0 ms. Thereafter, it remained suspended there as the Laplace pressure exceeded the gravity force under these conditions. From 0.6 to 1.2 ms, the droplet moved approximately 0.5 mm; therefore, the average velocity was approximately 0.833 m/s, which agrees well with the analytical results (Guo and Tang 2015; Lv et al. 2014). This velocity is large enough to jet out the droplet onto a substrate (Eggers and Villermaux 2008), suggesting that this type of pillar has potential use in 3D printing and other applications.
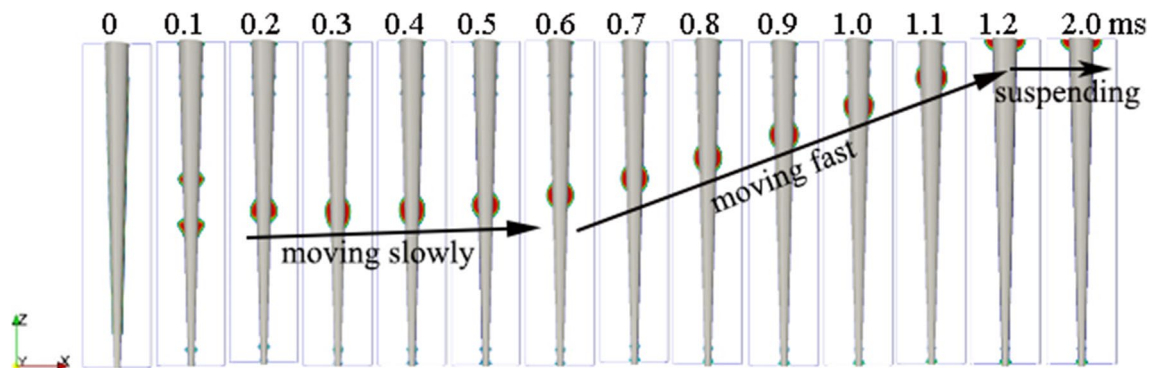
Fig. 3 Section view of the dynamic process of water droplet formation and transport. It consists of four stages: forming one droplet, moving slowly, moving quickly, and being suspended. The droplet velocity during the fast moving stage was about 0.833 m/s

2.2.2 Parameters optimization

In order to optimize the liquid transporting process, parametric studies using parameters such as geometry size, taper angle, and surface properties of the pillar were conducted.

2.2.2.1 Geometry size of pillar To study the effects of the shape of the substrate on the liquid being directionally transported, the diameter of the bottom end of the pillar was set at 10, 50, 80, 100, and 200 μm, while the taper angle was kept the same at 1.57°. The diameter of the top end was 65, 325, 520, 625, and 1300 μm, respectively. These dimensions are referenced as Cases 1–5, respectively. Other parameters such as the ratio of the initial liquid layer to pillar size, surface tension, and contact angle were kept the same as listed in Table 1.

The modeling results are shown in Fig. 4 and summarized in Table 2. It can be seen that when the pillar size was sufficiently small, the Laplace pressure component along the z-axis exceeded the gravity force and the droplet moved quickly to the top end of the pillar. When the size was increased by a factor of 5 as shown in Case 2, the Laplace pressure component along the z-axis was still larger than the gravity force, so the droplet could still be transported upward to the top end. However, when the pillar size was increased

Table 2 Summary of the effects of geometry size on droplet transporting

Cases	Diameter of the bottom end (μm)	Diameter of the top end (μm)	Results
1	10	65	Upward
2	50	325	Upward
3	80	520	Oscillating
4	100	625	Downward
5	200	1300	Downward

by a factor of 8 as shown in Case 3, the Laplace pressure component along the z-axis was almost as the same as the gravity force, so the droplet was oscillating but eventually reached the top end. When the pillar size was increased by a factor of 10 or more as shown in Case 4 and 5, respectively, the Laplace pressure component along the z-axis was no longer larger than the force of gravity: The droplet directly dropped down to the bottom end of the pillar. Therefore, it can be inferred that for a specific inverted tapered pillar, when its size is sufficiently small, the liquid can overcome the force of gravity and be transported upward spontaneously. The smaller size is also beneficial for transporting the liquid.

Fig. 4 Section view of final droplet location on the surface of inverted pillars in different sizes. The diameter of the bottom end of the pillar was set at 10, 50, 80, 100, and 200 μm for Cases 1–5, respectively. To make a good illustration and comparisons with other cases, the Cases 1 and 2 were magnified 1.5 times than the original ones, respectively. The taper angle was kept as 1.57°
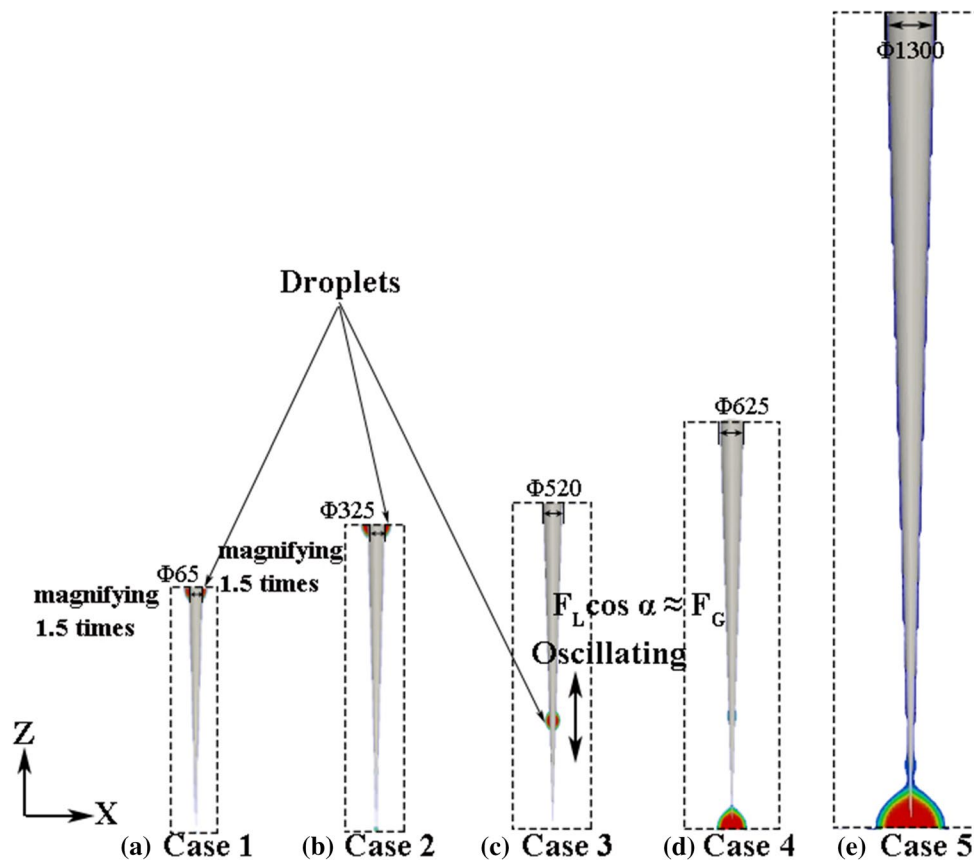
2.2.2.2 Taper angle of pillar To study the effect of the taper angle on the liquid directional transport, the taper angle of the pillar was set to 0, 0.785°, 1.57°, 5°, 10°, and 18°, while the diameter of the bottom end was kept constant at 10 μm. The diameter of the top end was set at 10, 37.4, 65, 185, 362.6, and 660 μm, respectively; these are referred to as Cases 1–6, respectively. Other parameters such as pillar length, the ratio of initial liquid layer to pillar size, surface tension, and contact angle were kept the same as those listed in Table 1.

The modeling results are shown in Fig. 5 and summarized in Table 3. It can be seen that when the taper angle was zero, the thin layer of water firstly turned into a few tiny droplets due the Rayleigh instability. As there was no curvature gradient, there was no Laplace pressure. Due to the tiny volume of each droplet, the gravity force acting on them was small; therefore, these tiny droplets could neither move upward nor drop downward but were suspended on the surface at the end of the calculated time limit, as shown in Case 1. When the taper angle increased to 0.785°, the Laplace pressure component along the z-axis was large enough to overcome the gravity force, so the droplet gradually moved upward and eventually reached the top end, as shown in Case 2.

As the taper angle (α) increased from 0° to 18°, the Laplace pressure (F_L, Eq. 1.1) increased correspondingly; however, the normalized component along the z-axis ($F_L\cos\alpha$) decreased, so their combination resulted in the droplet moving upward firstly as shown in Cases 3–4, but then dropping downward as shown in Cases 5–6.

Therefore, it can be inferred that for a specific liquid, there is only a narrow window of taper angles in an inverted tapered pillar that will successfully transport the liquid upward.

Table 3 Summary of the effects of taper angle on droplet transport

Cases	Taper angle (°)	Diameter of the bottom end (μm)	Diameter of the top end (μm)	Results
1	0	10	10	Suspending
2	0.785	10	37.4	Upward
3	1.57	10	65	Upward
4	5	10	185	Upward
5	10	10	362.6	Two droplets
6	18	10	660	Downward

2.2.2.3 Surface properties of pillar The contact angle is usually used to characterize the interface force between the pillar surface and liquid. Therefore, to study the effects of surface properties on the liquid droplet transport, the contact angle was set at 0°, 30°, 45°, 54.5°, 60°, and 90°, which are referenced as Cases 1–6, respectively. Other parameters such as pillar size, the ratio of initial liquid layer to pillar size, and surface tension were kept the same as listed in Table 1.

The modeling results are shown in Fig. 6 and summarized in Table 4. It can be seen that when the contact angle was smaller than 45° as shown in Cases 1–3, the Laplace pressure component along the z-axis always exceeded the gravity force; the droplet moved quickly to the top end of the pillar. However, when the contact angle increased to 54.5° as shown in Case 4, the Laplace pressure component along the z-axis was almost the same as the gravity force. Thus, a new balanced system was formed, such that the droplet was oscillating but could still eventually reach the top end. When the contact angle was continually increased to 60°, or even
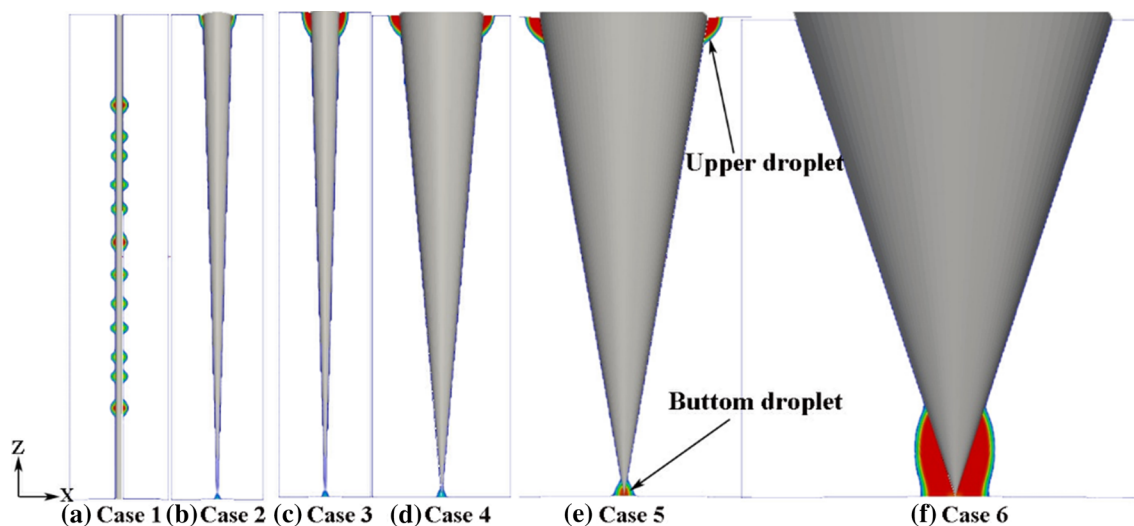
Fig. 5 Section view of final droplet location on the surface of inverted pillars with different taper angles. The taper angle of the pillar was set to 0°, 0.785°, 1.57°, 5°, 10°, and 18° for Cases 1–6, respectively. The diameter of the bottom end was kept at 10 μm

Fig. 6 Section view of final droplet location on the surface of inverted pillars of different wetting ability. The contact angle was set to 0°, 30°, 45°, 54.5°, 60°, and 90° for Cases 1–6, respectively
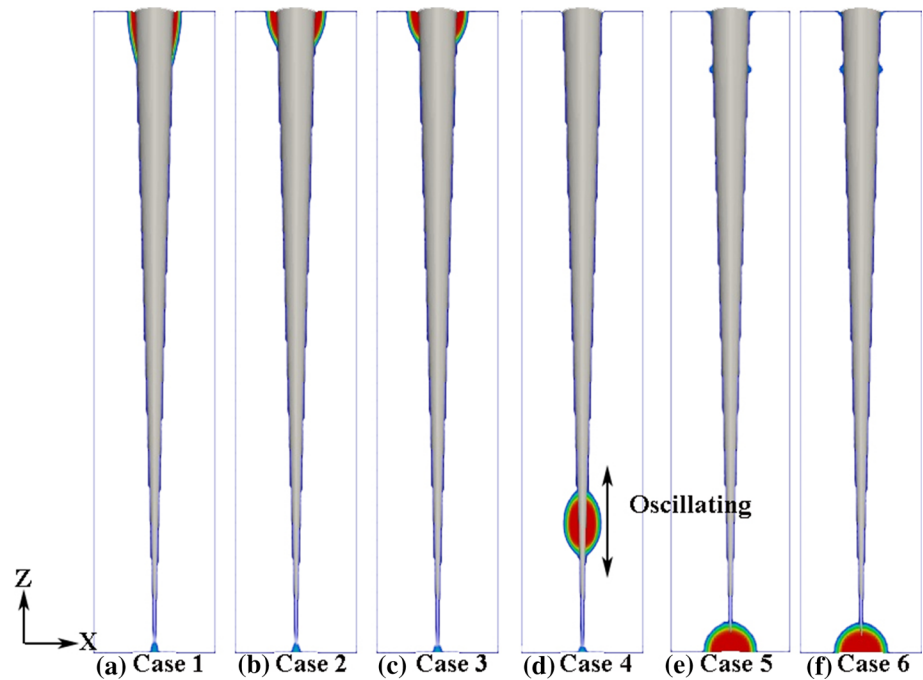
Table 4 Summary of the effects of contact angle on droplet transport

Cases	Contact angle (°)	Results
1	0	Upward
2	30	Upward
3	45	Upward
4	54.5	Oscillating
5	60	Downward
6	90	Downward

larger to 90°, as shown in Cases 5 and 6, respectively, the Laplace pressure component along the z-axis was no longer larger than the force of gravity: The droplet then dropped down to the bottom end of the pillar. Therefore, it can be inferred that for a specific type of liquid, a small contact angle means that the surface of the pillar is hydrophilic and is thus beneficial for transporting liquid.

From the above modeling study, it can be concluded that when the taper angle of the pillar is less than 10°, the diameter of its bottom end is less than 80 μm, and the contact angle of liquid on the pillar surface is less than 54.5°, the liquid may be transported upward spontaneously.

3 Fabricating experiments

3.1 Tapered pillar fabrication

In order to verify the modeling results, a series of experiments were conducted. Previous studies demonstrated that the gradient electrochemical corrosion method can fabricate tapered pillars with various geometry shapes (Ju et al. 2013; Wang et al. 2014). However, the typical contact angle of water on a regular copper surface is approximately 90° (Ju et al. 2013), which is out of range of spontaneously transporting liquid upward on a copper surface. Fortunately, some other researchers have developed methods to improve the wettability of water on the copper surface and can change the contact angle from 90.3° to 0°(Li and Thoroddsen 2013; Tong et al. 2015), which perfectly matches the desired contact angle from the simulation results. Therefore, the copper wire was chosen to fabricate the inverted tapered pillar.

The commercial copper wires used in the experiment were purchased from Jinjia Metal Material Co., Ltd, China, with a diameter of 0.3 mm. The commercial copper wire was polished carefully with sandpaper, cleaned in 1.0 M HCl aqueous solution for 5 min under ultrasonication condition, and dried by pure dry air flow before experiments. Afterward, the wire was fixed vertically on a programmable linear motor (manufactured by Shenzhen Tech-D Precision Automation Co., Ltd with the resolution of z-axis motion in 1 μm). And one of the wire ends was connected to the anode of a 5 V DC power supply (E3634A, Keysight), while the other end was immersed in the electrolyte solution. The electrolyte was the aqueous solution containing $CuSO_4$ (0.2 M). A clean copper sheet (20 mm × 20 mm), connecting to the cathode of the power supply, was also immersed in the electrolyte solution, as shown in Fig. 7a. When the linear motor periodically moved in the z-axis direction, it brought the copper wire raising and falling together which made the

Fig. 7 Tapered pillar fabricating experiment. **a** Fabricating experiment setup which is consisted of a programmable linear motor with high precision and an electrochemical system. The beaker was filled with the aqueous solution with $CuSO_4$ (0.2 M). **b** One of the tapered pillars fabricated by gradient electrochemical corrosion and electrochemical modification. The α equals to 5.65°. The scale bar is 500 μm
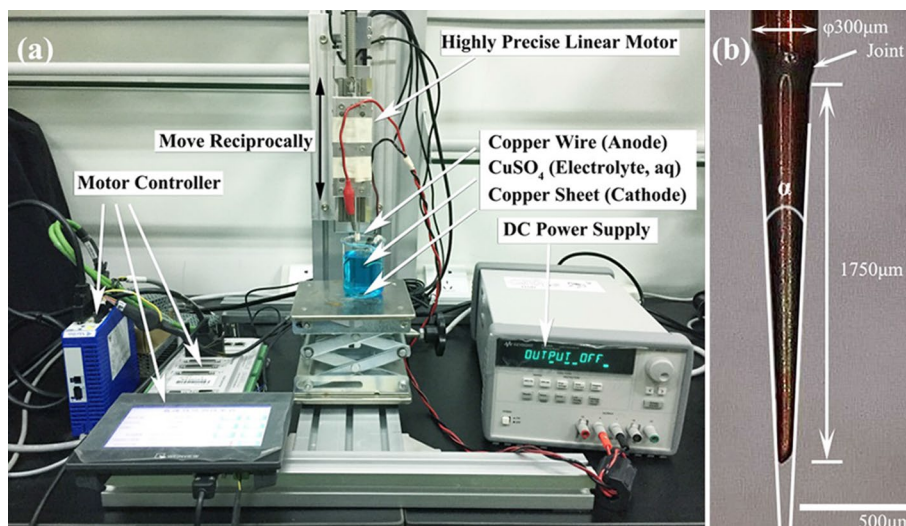
electrochemical corrosion time varying along its height; thus, a tapered pillar was fabricated, as shown in Fig. 7b.

From the modeling results in Sect. 2, it is known that the tiny droplet cannot spontaneously move from the tip to the top on a tapered pillar surface when the contact angle of liquid is greater than 54.4°, which is also confirmed by our experiments. Thus, to enhance the wetting ability of the copper pillar, the electrochemical modification method was used. The copper-tapered pillar was kept connecting with the anode of the DC power supply, but the voltage was lowered to be 1 V. And the electrolyte was replaced by the aqueous solution containing KOH (3 M). The clean copper sheet was kept connecting to the cathode of the power supply and immersing in the electrolyte solution. The programmable linear motor was then used to preciously control the length of the tapered pillar immersed in the electrolyte solution. Thus, $Cu(OH)_2$ nanoribbon was grown upon the surface during this electrochemical modification process, therefore, reducing the contact angle of water on the copper-tapered pillar (Cheng et al. 2015).

## 3.2 Liquid transporting experiments and discussions

An experimental setup was used to monitor the liquid transport process, as shown in Fig. 8. It consists of a tapered pillar, a homemade gripper, a syringe, and a camera system. The high-speed camera is VW-600C (manufactured by Keyence) with a high-intensity light for clear imaging. It can work at a high speed (1000 frames per second) and high resolution (640 × 480 pixels). The tapered pillar was vertically fixed by the homemade gripper. The high-precision syringe (manufactured by Hamilton) equipped with a tiny needle (outer diameter 0.24 mm, purchased from Puyasi Commercial Trading Co., Ltd) was used to inject a small
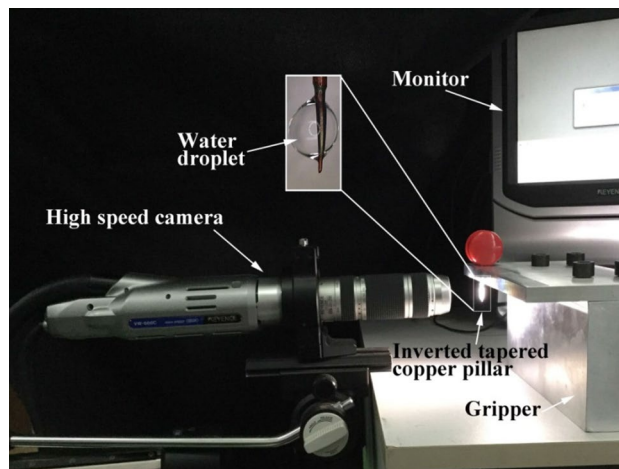

Fig. 8 Experimental setup for water transporting. It consists of a tapered pillar, a homemade gripper, a syringe pump, and a camera system

amount of deionized water and then place it on the tip of the copper-tapered pillar. Both the temperature (25 °C) and humidity (45%) were carefully controlled to minimize the effects of the environment.

During the experiment, after the small droplet was placed on the tip of the pillar, the high-speed camera was turned on simultaneously to record the whole transporting process, as shown in Fig. 9. From 0 to 10 ms, the small droplet moved upward to 0.609 mm. The average velocity was approximately 60.9 mm/s. As the droplet is much bigger than the one modeled in Sect. 2 (the diameter of the droplet is 1020 μm, and thus the volume can be calculated as 0.56 μL), the gravity force is larger, and thus the transporting velocity is relatively small. From 10 to 210 ms, the upper part of the droplet went beyond the tapered pillar and reached the joint.
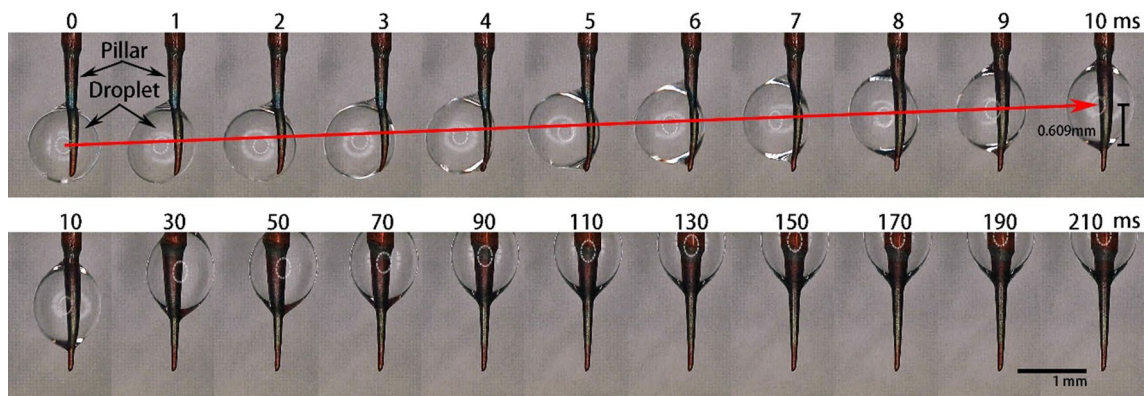
Fig. 9 Experimental results of water transporting process. From 0 to 10 ms, a small droplet moved upward against the gravity on the surface of the tapered pillar. From 10 to 210 ms, the upper part of the droplet went beyond the tapered pillar and reached the joint. Scale bar is 1 mm
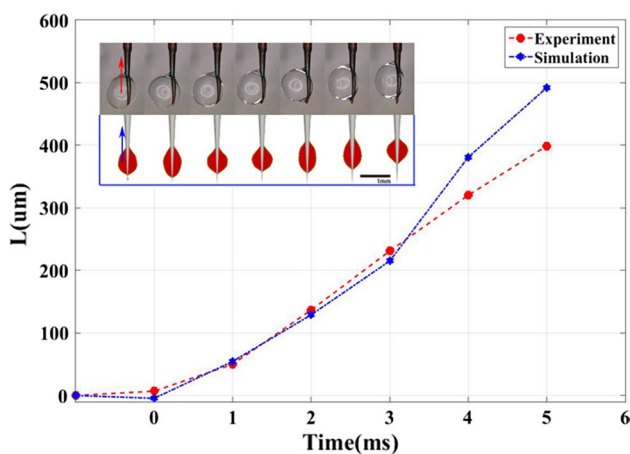
Fig. 10 Comparisons between the modeling and the experimental results. It can be clearly noted that the simulated results agree well with the experimental ones

Finally, it stopped near the joint due to the balance between the Laplace pressure and the gravity.

To further verify the model, the corresponding conditions were used in the model. The relationship between the displacement of the droplet and time was obtained and compared with those extracted from the recorded video, as shown in Fig. 10. It can be clearly noted that the simulated results agree well with the experimental ones which demonstrates the correctness of the model.

4 Conclusion

In this paper, the possibility of spontaneously transporting a droplet upward along an inverted tapered pillar was theoretically analyzed and a numerical model was developed to design such inverted tapered pillars. Using this model, the dynamic process of the transporting liquid was simulated and a range of acceptable parameters for the pillar's geometry was obtained. When the taper angle, the diameter of the bottom end of the pillar, and the contact angle of liquid are less than 10°, 80 µm, and 54.5°, respectively, the liquid may be spontaneously transported upward. To fabricate the designed pillar, an experimental setup was also developed. With the setup, the designed pillar was successfully fabricated by the gradient electrochemical corrosion method and enhanced its wettability by the electrochemical modification method. The fabricated pillar was then experimentally validated showing that it can spontaneously transport a microsize droplet upward. In conclusion, this paper provides a new and systematic way to design and fabricate a tool for liquid transport with high efficiency.

Authors' contributions Y.C carried out the experiments and drafted the manuscript. D.S, X.M, and L.L helped the experiments. J.G, X.C, H.L, and C.P.W contributed to the principal aspects and supervised the progress of the research. All authors reviewed the manuscript.

Compliance with ethical standards

Conflict of interest The authors declare that they have no competing interests.

References

Basaran OA, Suryo R (2007) Fluid dynamics: the invisible jet. Nat Phys 3(10):679–680

Bico J, Quéré D (2002) Self-propelling slugs. J Fluid Mech 467:101–127

Chen Y, Guo M, Yang K, Wang C (2013) Enhanced cooling for LED lighting using ionic wind. Int J Heat Mass Transf 57(1):285–291

Cheng J, Sun Y, Zhao A, Huang Z, Xu S (2015) Preparation of gradient wettability surface by anodization depositing copper hydroxide on copper surface. Trans Nonferr Met Soc 25(7):2301–2307

Chu PK, Liu X (2008) Biomaterials fabrication and processing handbook. CRC Press, Boca Raton

Dai Q, Khonsari MM, Shen C, Huang W, Wang X (2016) Thermocapillary migration of liquid droplets induced by a unidirectional thermal gradient. Langmuir 32(30):7485–7492

Eggers J, Villermaux E (2008) Physics of liquid jets. Rep Prog Phys 71(3):36601

Ferraro P, Coppola S, Grilli S, Paturzo M, Vespini V (2010) Dispensing nano-pico droplets and liquid patterning by pyroelectrodynamic shooting. Nat Nanotechnol 5(6):429–435

Guo L, Tang GH (2015) Experimental study on directional motion of a single droplet on cactus spines. Int J Heat Mass Transf 84:198–202

Guo MT, Rotem A, Heyman JA, Weitz DA (2012) Droplet microfluidics for high-throughput biological assays. Lab Chip 12(12):2146–2155

Huang JY, Lo Y, Niu JJ, Kushima A, Qian X, Zhong L, Mao SX, Li J (2013) Nanowire liquid pumps. Nat Nanotechnol 8(4):277–281

Ju J, Bai H, Zheng Y, Zhao T, Fang R, Jiang L (2012) A multi-structural and multi-functional integrated fog collection system in cactus. Nat Commun 3:1247

Ju J, Xiao K, Yao X, Bai H, Jiang L (2013) Bioinspired conical copper wire with gradient wettability for continuous and efficient fog collection. Adv Mater 25(41):5937–5942

Ju J, Zheng Y, Jiang L (2014) Bioinspired one-dimensional materials for directional liquid transport. Acc Chem Res 47(8):2342–2352

Katsikis G, Cybulski JS, Prakash M (2015) Synchronous universal droplet logic and control. Nat Phys 11:588–597

Li EQ, Thoroddsen ST (2013) The fastest drop climbing on a wet conical fibre. Phys Fluids (1994-present) 25(5):52105

Li K, Ju J, Xue Z, Ma J, Feng L, Gao S, Jiang L (2013) Structured cone arrays for continuous and effective collection of micron-sized oil droplets from water. Nat Commun 4:2276

Li J, Wang D, Duan JA, He H, Xia Y, Zhu W (2015) Structural design and control of a small-MRF damper under 50 N soft-landing applications. IEEE Trans Ind Inform 11(3):612–619

Li J, Zhang X, Zhou C, Zheng J, Ge D, Zhu W (2016) New applications of an automated system for high-power LEDs. IEEE-ASME Trans Mech 21(2):1035–1042

Liang Y, Tsao H, Sheng Y (2015) Drops on hydrophilic conical fibers: gravity effect and coexistent states. Langmuir 31(5):1704–1710

Lorenceau É, Quéré D (2004) Drops on a conical wire. J Fluid Mech 510:29–45

Luo C (2015) Theoretical exploration of barrel-shaped drops on cactus spines. Langmuir 31(43):11809–11813

Lv C, Chen C, Chuang Y, Tseng F, Yin Y, Grey F, Zheng Q (2014) Substrate curvature gradient drives rapid droplet motion. Phys Rev Lett 113(2):26101

Madou MJ (2011) Manufacturing techniques for microfabrication and nanotechnology, vol 2. CRC Press, Boca Raton

Michielsen S, Zhang J, Du J, Lee HJ (2011) Gibbs free energy of liquid drops on conical fibers. Langmuir 27(19):11867–11872

Park K, Kim P, Grinthal A, He N, Fox D, Weaver JC, Aizenberg J (2016) Condensation on slippery asymmetric bumps. Nature 531(7592):78–82

Price AK, Paegel BM (2016) Discovery in droplets. Anal Chem 88(1):339–353

Rowlinson JS, Widom B (2013) Molecular theory of capillarity. Courier Corporation, Chelmsford

Subramanian RS, Moumen N, McLaughlin JB (2005) Motion of a drop on a solid surface due to a wettability gradient. Langmuir 21(25):11844–11849

Tong WL, Tan MK, Chin JK, Ong KS, Hung YM (2015) Coupled effects of hydrophobic layer and vibration on thermal efficiency of two-phase closed thermosyphons. RSC Adv 5(14):10332–10340

Vorobyev AY, Guo C (2009) Metal pumps liquid uphill. Appl Phys Lett 94(22):224102

Wang Q, Meng Q, Chen M, Liu H, Jiang L (2014) Bio-inspired multistructured conical copper wires for highly efficient liquid manipulation. ACS Nano 8(9):8757–8764

Wang Q, Meng Q, Liu H, Jiang L (2015) Chinese brushes: From controllable liquid manipulation to template-free printing microlines. Nano Res 8(1):97–105

Wu S, Yang C, Hsu W, Lin L (2015) 3D-printed microelectronics for integrated circuitry and passive wireless sensors. Microsyst Nanoeng 1:1–9

Yuan Y, Lee TR (2013) Contact angle and wetting properties. Springer, Berlin

Zheng Y, Bai H, Huang Z, Tian X, Nie F, Zhao Y, Zhai J, Jiang L (2010) Directional water collection on wetted spider silk. Nature 463(7281):640–643

Zhu H, Guo Z, Liu W (2016) Biomimetic water-collecting materials inspired by nature. Chem Commun 52(20):3863–3879